IMA Journal of Applied Mathematics (2021) **86**, 984–1009
https://doi.org/10.1093/imamat/hxab030
Advance Access publication on 26 July 2021

Spatial localization beyond steady states in the neighbourhood of the Takens–Bogdanov bifurcation

HAIFAA ALRIHIELI
School of Mathematics, University of Leeds, Leeds LS2 9JT, UK, and Faculty of Science, University of Tabuk, Tabuk 47512, Saudi Arabia

ALASTAIR M. RUCKLIDGE
School of Mathematics, University of Leeds, Leeds LS2 9JT, UK

AND

PRIYA SUBRAMANIAN*
Mathematical Institute, University of Oxford, Oxford OX2 6GG, UK
*Corresponding author: priya.subramanian@maths.ox.ac.uk

[Received on 1 October 2020; revised on 16 April 2021; accepted on 10 June 2021]

Double-zero eigenvalues at a Takens–Bogdanov (TB) bifurcation occur in many physical systems such as double-diffusive convection, binary convection and magnetoconvection. Analysis of the associated normal form, in 1D with periodic boundary condition, shows the existence of steady patterns, standing waves, modulated waves (MW) and travelling waves, and describes the transitions and bifurcations between these states. Values of coefficients of the terms in the normal form classify all possible different bifurcation scenarios in the neighbourhood of the TB bifurcation (Dangelmayr, G. & Knobloch, E. (1987) The Takens–Bogdanov bifurcation with O(2)-symmetry. Phil. Trans. R. Soc. Lond. A, **322**, 243-279). In this work we develop a new and simple pattern-forming partial differential equation (PDE) model, based on the Swift–Hohenberg equation, adapted to have the TB normal form at onset. This model allows us to explore the dynamics in a wide range of bifurcation scenarios, including in domains much wider than the lengthscale of the pattern. We identify two bifurcation scenarios in which coexistence between different types of solutions is indicated from the analysis of the normal form equation. In these scenarios, we look for spatially localized solutions by examining pattern formation in wide domains. We are able to recover two types of localized states, that of a localized steady state (LSS) in the background of the trivial state (TS) and that of a spatially localized travelling wave (LTW) in the background of the TS, which have previously been observed in other systems. Additionally, we identify two new types of spatially localized states: that of a LSS in a MW background and that of a LTW in a steady state (SS) background. The PDE model is easy to solve numerically in large domains and so will allow further investigation of pattern formation with a TB bifurcation in one or more dimensions and the exploration of a range of background and foreground pattern combinations beyond SSs.

Keywords: pattern formation; Takens–Bogdanov bifurcation; spatial localization.

1. Introduction

The Takens–Bogdanov (TB) bifurcation exhibits a variety of dynamical behaviours and occurs when a Hopf bifurcation and a pitchfork bifurcation coincide. More precisely, this bifurcation occurs when there is a double zero eigenvalue (algebraic multiplicity two) but only a single eigenvector (geometric multiplicity one). For nearby parameter values we can identify two co-dimension 1 bifurcations, a Hopf and pitchfork bifurcation. The loci of the Hopf bifurcation ends at the TB point. Such a situation arises in diverse fluid flow situations such as in double-diffusive convection in a horizontal layer of fluid heated from below (Knobloch & Proctor, 1981; Rucklidge, 1992), in magnetoconvection (Dawes, 2000) and in pipe flow (Mellibovsky & Eckhardt, 2011) to name a few.

In this work, we start with the case of double-diffusive convection where two competing gradients that drive motion in the fluid: the temperature gradient and the solute gradient. With low solute gradient, the first bifurcation from the resting (trivial) state as the temperature gradient is increased is a pitchfork bifurcation leading to steady convection. With larger solute gradient, the bifurcation changes to a Hopf bifurcation leading to oscillatory convection. In double-diffusive convection with idealized boundary conditions, these two forms of convection set in with the same horizontal wavelength (Veronis, 1965). In 2D with periodic boundary conditions the point where we have two zero eigenvalues with algebraic multiplicity of two but geometric multiplicity one is called the TB point. The normal form that describes the amplitude close to the TB point for a system with O(2) symmetry is (Dangelmayr & Knobloch, 1987)

$$\ddot{z} = \mu z + A|z|^2 z + \epsilon\left(\nu\dot{z} + C\left(\dot{z}\bar{z} + z\dot{\bar{z}}\right)z + D|z|^2\dot{z}\right) + O(\epsilon^2), \qquad \epsilon \ll 1, \tag{1.1}$$

where z is the complex amplitude of the pattern; μ and ν are the unfolding parameters; A, C and D are constants; the dot denotes differentiation with respect to time; and ϵ controls how close the system is to the TB point. The pattern itself is given by functions of the form $z(t)e^{ix} + \bar{z}(t)e^{-ix}$.

Different bifurcation scenarios obtained by the analysis of the amplitude equation are found close to onset (Dangelmayr & Knobloch, 1987; Knobloch, 1986), with several different types of patterns: steady states (SSs), travelling waves (TWs), standing waves (SWs) and modulated waves (MWs). In domains that are many times wider than the preferred wavelength, extended TW, SW and MW solutions have been found in numerical investigations of the partial differential equations (PDEs) for thermosolutal convection (Deane *et al.*, 1988; Spina *et al.*, 1998; Turton *et al.*, 2015). In a similar scenario, in binary convection, the application of a thermal gradient to a mixture sets up a competing concentration gradient due to the Soret effect. In this system, a transition from SS to TW has been observed in numerical simulations (Barten *et al.*, 1995a; Zhao & Tian, 2015), while a nonlinear SW solution has been numerically obtained by Matura *et al.* (2004) and Jung *et al.* (2004).

In addition to patterned states that are spatially extended, i.e. span the entire domain, parameter values where both the trivial state (TS) and a periodic SS state are both dynamically stable allow for the existence of spatially localized states. In the subcritical regime with coexistence between the TS and the periodic SS branches, spatially localized steady states (LSSs) in a background of the TS undergoing homoclinic snaking have been obtained in numerical investigations of thermosolutal convection (Beaume *et al.*, 2011) and binary convection (Batiste *et al.*, 2006; Mercader *et al.*, 2009). The snaking branches behave like those familiar from the Swift–Hohenberg equation (Burke & Knobloch, 2007). At a given Rayleigh number, odd and even branch solutions with different number of rolls can be found.

For binary convection, the system undergoes a subcritical Hopf bifurcation to TW for negative separation ratio (Zhao & Tian, 2015). In the parameter regime where the TW bifurcate subcritically from the conduction state, localized travelling waves (LTWs) have also been obtained. The LTW solution refers to the spatially localized cells whose envelope moves with a characteristic speed in a background of the TS. In contrast to LSS, the LTW have fixed and uniquely selected width, which was discovered in experimental (Kolodner, 1991a,c, 1994; Niemela *et al.*, 1990) and numerical (Barten *et al.*, 1991, 1995b; Taraut *et al.*, 2012) studies of binary convection, with a negative separation ratio $= -0.08$. This was

TABLE 1 *Families of equilibria. The states SS, TW, SW and MW are periodic patterns that fill the domain. The last four are localized patterns of one type in the background of another. Examples of each of these are given in the named figures*

Acronym	Name	Conditions in (1.2)	Figure references
TS	Trivial state	$r = 0$ and $L = 0$	
SS	Steady state	$r > 0$ and $\dot{r} = s = L = \dot{L} = 0$	
TW	Traveling wave	$r > 0,\ L \neq 0$ and $\dot{r} = s = \dot{L} = 0$	
SW	Standing wave	$L = 0$ and $\dot{r} \neq 0$	
MW	Modulated wave	$L \neq 0$ and $\dot{r} \neq 0$	
LSS-TS	Localized SS in TS background		Fig. 5(*a*)
LSS-MW	Localized SS in MW background		Fig. 5(*b*)
LTW-TS	Localized TW in TS background		Fig. 9
LTW-SS	Localized TW in SS background		Fig. 10

also observed later in numerical simulations of the full system of binary convection with different but still small negative separation ratios of -0.123 (Watanabe *et al.*, 2012) and -0.1 (Zhao & Tian, 2015).

In order to discuss different families of possible solutions for the system given in (1.1) we use the transformation $z = r\exp(i\phi)$, along with the relations $s = \dot{r}$ and $L = r^2\dot{\phi}$, to get a 3D system with the variables (r, s, L) equivalent to (1.1). The evolution equations for this system then become

$$
\begin{aligned}
\dot{r} &= s, \\
\dot{s} &= \mu r + Ar^3 + \frac{L^2}{r^3} + \epsilon\left(\nu + Mr^2\right)s + O(\epsilon^2), \\
\dot{L} &= \epsilon\left(\nu + Dr^2\right)L + O(\epsilon^2).
\end{aligned}
\tag{1.2}
$$

In terms of this 3D system, we can identify the different families of solutions using the conditions shown in Table 1, where we also define names for several localized patterns. Non-drifting patterns (SS, SW) have z with constant phase, whereas drifting patterns have phases that vary over time.

In this paper, we develop a new and simple model as a useful description of the qualitative features of double-diffusive convection. Our model is a PDE based on the Swift–Hohenberg equation but adapted to have the TB normal form at onset. This allows for an exploration of the dynamics of localized steady and time dependent patterns in very wide domains. Our model can access most of the bifurcation scenarios that occur in the TB normal form and so it is relevant to other pattern-forming systems whose dynamics can be reduced to a TB normal form.The model recovers LSS and LTW as documented above, as well as two new localized patterns: LSS in an oscillating background and LTW moving through a background of SS.

In Section 2, we develop the linear part of the model by reproducing the dynamics of double-diffusive convection. In Section 3, we discuss the nonlinearities which we can add to the model, taking into account Lyapunov stability. In Section 4, the model is reduced to the TB normal form by applying a weakly nonlinear analysis. In Section 5, we identify parameter combinations in the model at which we can observe different dynamical behaviours close to the TB bifurcation. In Section 6, we obtain localized SS with TS background and localized SS with SW background using time stepping and observe snaking

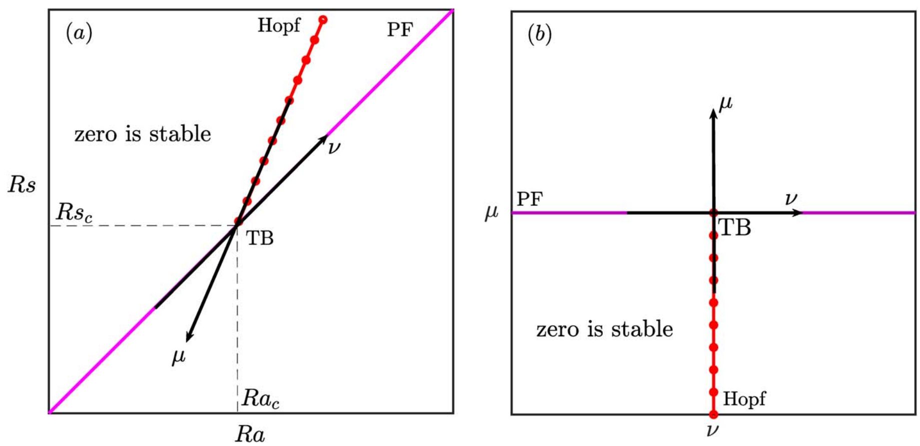

FIG. 1. (*a*) Schematic unfolding diagram for the pitchfork (PF, pink solid line) and Hopf (red line with circle markers) in the (Ra, Rs)-plane of double-diffusive convection. The line of Hopf bifurcations ends at the co-dimension two TB with $(Ra, Rs) = (Ra_c, Rs_c)$. For each Rs, the quiescent/zero state is stable at small values of Ra until we cross either a pitchfork/Hopf transition as we increase Ra. (*b*) The (ν, μ)-plane mapped from (*a*).

in the branch of localized SS with TS background using continuation. Localized TW with TS and SS background are discussed in Section 7 using time stepping. We conclude in Section 8.

2. Designing the linear dynamics near the TB bifurcation

The first part of designing a model system that has a Takens–Bogdanov (TB) bifurcation requires the possibility for both a pitchfork and a Hopf bifurcation. We build a minimal model for the TB bifurcation by reproducing the dynamics of double-diffusive convection, starting with the design of the linear dynamics. Two different density gradients drive the dynamics in double-diffusive convection: thermal gradients quantified with a thermal Rayleigh number Ra and solutal gradients quantified with a solutal Rayleigh number Rs. The stable quiescent state in the system becomes unstable with increasing thermal gradients and starts to convect. When Rs is less than a critical value Rs_c, the quiescent state undergoes a pitchfork bifurcation leading to steady convection as the temperature gradient Ra increases. At large solutal gradients with $Rs > Rs_c$, this behaviour changes and the quiescent state loses stability via a Hopf bifurcation leading to oscillatory convection. The point where the primary bifurcation changes from pitchfork to Hopf bifurcation with $(Ra, Rs) = (Ra_c, Rs_c)$ is called the Takens–Bogdanov point, as shown in Fig. 1(*a*).

In order to replicate this behaviour, we use two control parameters ν and μ in the new model, where the change of sign in ν corresponds to the loci of pitchfork bifurcations and the change of sign in μ (with $\nu < 0$) corresponds to the loci of Hopf bifurcations, as shown schematically in Fig. 1(*b*). Such an identification allows us to decompose the behaviour close to the TB point as follows. Starting from ν and μ both negative, increasing ν and μ together, parallel to but above the diagonal $\nu = \mu$ leads to a pitchfork bifurcation at $\mu = 0$ with $\nu < 0$. Increasing ν and μ together below the diagonal leads to first a Hopf bifurcation at $\nu = 0$ with $\mu < 0$, then a pitchfork bifurcation at $\mu = 0$ with $\nu > 0$. In this way we are able to replicate the different bifurcation scenarios from double-diffusive convection.

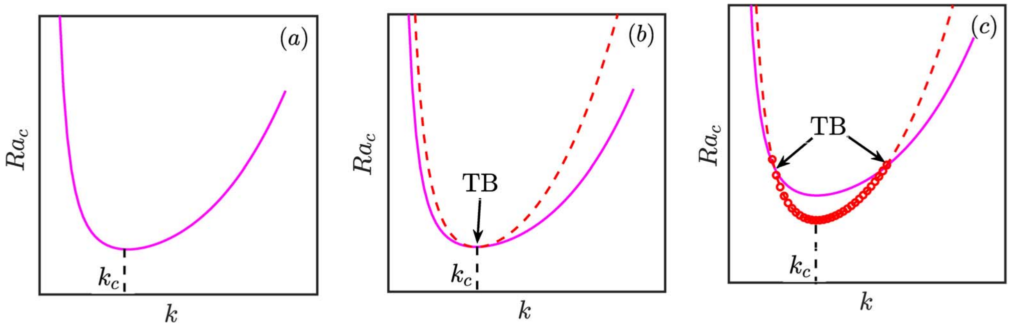

FIG. 2. Schematic plot of the neutral stability curves for pitchfork and Hopf bifurcation for double-diffusive convection showing the critical Rayleigh number as a function of wavenumber k. The pink solid line refers to the loci of pitchfork bifurcation. The red circle markers identify locations where the Hopf bifurcation is the primary bifurcation. On the red dashed line without circle markers, the amplitude equations has two real eigenvalues that add up to zero. (*a*) $Rs < Rs_c$ where pitchfork bifurcations are the primary bifurcation, (*b*) $Rs = Rs_c$ where the pitchfork and Hopf bifurcation thresholds meet at a TB point and (*c*) $Rs > Rs_c$ where the pitchfork and Hopf bifurcation can be primary bifurcations. In this case two TB points can be identified. The minima of the curves define the critical wavenumber and Rayleigh number. In the double-diffusion case, the wavenumbers are the same for both the pitchfork and Hopf bifurcations in (*c*).

The second factor to include is the variation of the linear stability threshold with wavenumber k. In the case of double-diffusive convection, the linear stability thresholds for pitchfork and Hopf bifurcations are as shown in Fig. 2. In all three cases, we observe that both the pitchfork and Hopf thresholds vary with the wavenumber k. For example, the threshold for pitchfork bifurcations (shown in pink) has a minimum $Ra = Ra_0$ at $k = k_c$. Near this critical wavenumber k_c, the critical Rayleigh number varies with the square of the distance of the current wavenumber k from k_c. This means that close to $k = k_c$, Ra_0 can be expanded as

$$Ra_0(k^2) \approx Ra_0 + \frac{Ra_0''}{8k_c^2}(k_c^2 - k^2)^2, \tag{2.1}$$

where $Ra_0'' = d^2Ra_0/dk^2$. In order to reproduce this behaviour in the new model, we incorporate such a variation into the two linear stability thresholds by writing μ and ν in terms of $(k_c^2 - k^2)^2$ as

$$\begin{aligned} \mu &= (k_{\mathrm{cPF}}^2 - k^2)^2, \\ \nu &= b(k_{\mathrm{cHopf}}^2 - k^2)^2\,. \end{aligned} \tag{2.2}$$

Here the constant b is used to change the rate at which Hopf bifurcation varies with $(k_c^2 - k^2)^2$. From the case of double diffusion shown in Fig. 2, we see that we require $b > 1$. Other choices can be made depending on the specific system of interest.

Close to the TB point, the PDEs that govern small amplitude thermosolutal convection can be reduced to the linear second order Van der Pol–Duffing equation (Veronis, 1965)

$$\ddot{u} - \kappa\dot{u} - \lambda u = 0, \tag{2.3}$$

where u is the amplitude of the lowest-order mode of the stream function, κ and λ are unfolding parameters and the dot indicates the derivative with respect to time. We start with this dynamical equation and look to fit in our two parameters in terms of the unfolding parameters in this model below.

For the linear equation in (2.3), we can assume a solution of the form $u = e^{\sigma t}$, where σ is the growth rate. The characteristic equation then takes the following form

$$\sigma^2 - \kappa\sigma - \lambda = 0. \tag{2.4}$$

This is equivalent to an eigenvalue problem for σ of the form

$$\sigma \begin{bmatrix} 1 \\ \sigma \end{bmatrix} = \begin{bmatrix} 0 & 1 \\ \lambda & \kappa \end{bmatrix} \begin{bmatrix} 1 \\ \sigma \end{bmatrix} \equiv \mathbf{L} \begin{bmatrix} 1 \\ \sigma \end{bmatrix}. \tag{2.5}$$

A pitchfork bifurcation (with one zero eigenvalue) occurs when the determinant is zero, i.e. $\lambda = 0$, and a Hopf bifurcation (with purely imaginary eigenvalues) occurs when the trace is zero and the determinant is positive, i.e. $\kappa = 0$ and $\lambda < 0$. At the TB point, the system has two zero eigenvalues, i.e. $\kappa = \lambda = 0$. We can relate μ and ν from Eqn. (2.2) to this 2D dynamical system by setting

$$\begin{aligned} \lambda &= \mu - (k_{\mathrm{cPF}}^2 - k^2)^2, \\ \kappa &= \nu - b(k_{\mathrm{cHopf}}^2 - k^2)^2 . \end{aligned} \tag{2.6}$$

This gives the relations that $\lambda = 0$ when $\mu = (k_{\mathrm{cPF}}^2 - k^2)^2$, and $\kappa = 0$ when $\nu = b(k_{\mathrm{cHopf}}^2 - k^2)^2$. This implies that the linear operator in terms of (2.6) is then given as

$$\mathbf{L} = \begin{bmatrix} 0 & 1 \\ \mu - (k_{\mathrm{cPF}}^2 - k^2)^2 & \nu - b(k_{\mathrm{cHopf}}^2 - k^2)^2 \end{bmatrix}. \tag{2.7}$$

Consequently, we can write the linear equation (2.3) as

$$\ddot{u} - \left(\nu - b(k_{\mathrm{cHopf}}^2 - k^2)^2\right)\dot{u} - \left(\mu - (k_{\mathrm{cPF}}^2 - k^2)^2\right)u = 0, \tag{2.8}$$

where $u(t)$ is now the amplitude at lowest order of the mode e^{ikx}. This equation in Fourier space can be converted into a PDE by replacing k^2 with $-\partial^2/\partial x^2$ and considering u to be a function of x and t. The ODE (2.8) converted to a PDE is

$$u_{tt} - \left(\nu - b\left(k_{\mathrm{cHopf}}^2 + \frac{\partial^2}{\partial x^2}\right)^2\right)u_t - \left(\mu - \left(k_{\mathrm{cPF}}^2 + \frac{\partial^2}{\partial x^2}\right)^2\right)u = 0, \tag{2.9}$$

where $u_{tt} = \partial^2 u/\partial t^2$ and $u_t = \partial u/\partial t$ are the derivatives with respect to time and the parameters k_{cPF} and k_{cHopf} are the critical wavenumbers for the pitchfork and Hopf bifurcations.

The general choice of $k_{\mathrm{cPF}} \neq k_{\mathrm{cHopf}}$ is relevant to problems where the pitchfork and Hopf bifurcation have different critical wavenumbers, e.g. magnetoconvection (Arter, 1983; Chandrasekhar, 1961; Proctor & Weiss, 1982; Weiss, 1981) and rotating convection (Clune & Knobloch, 1993; Veronis, 1966, 1968; Zimmermann *et al.*, 1988). In such cases, the TB point occurs at Rayleigh numbers above the critical value and therefore can be harder to access. Of course enforcing a wavenumber through a choice of domain size can allow us to reach the TB point. However, the solutions obtained in such an analysis might not persist in a larger extended domain, i.e. without an enforced wavenumber.

Since we are interested in thermosolutal convection, where the pitchfork and Hopf bifurcations have the same critical wavenumbers, for this paper we let $k_{\mathrm{cPF}} = k_{\mathrm{cHopf}} = 1$. Then the linear second order partial differential equation that models the dynamics at small amplitudes near a TB point takes the following form:

$$u_{tt} = \left(\nu - b\left(1 + \frac{\partial^2}{\partial x^2}\right)^2\right)u_t + \left(\mu - \left(1 + \frac{\partial^2}{\partial x^2}\right)^2\right)u \equiv \mathscr{M}_1 u + \mathscr{M}_2 u_t = 0. \tag{2.10}$$

The dispersion relation can be determined by studying the eigenvalues of the model given by

$$\sigma(k) = \frac{\left(\nu - b\left(1-k^2\right)^2\right) \pm \sqrt{\left(\nu - b\left(1-k^2\right)^2\right)^2 + 4\left(\mu - \left(1-k^2\right)^2\right)}}{2}. \tag{2.11}$$

The growth rate σ is a function of the wavenumber k, so some modes could decay and while others can grow. If the eigenvalues for all k have negative real parts the evolution decays and the zero solution is linearly stable. If any eigenvalue for any k has positive real part the evolution grows and the zero solution is linearly unstable.

3. Selection of the nonlinear terms

The model given in (2.10) is a second-order linear partial differential equation in time, which has been designed to reproduce the linear stability results of double-diffusive convection. This section deals with determining the choice of nonlinear terms in the model, with two aims: first, to have a globally stable nonlinear dynamical system; and second, to be able to access the variety of dynamical behaviours that can occur in the neighbourhood of the TB bifurcation.

We consider only those nonlinearities that are invariant with respect to reflection about the x-axis (to replicate this symmetry in double-diffusive convection) and include nonlinearities both in the field u and its time derivative u_t. We can additionally classify the nonlinear terms in the order at which they contribute to the dynamics. For example, quadratic nonlinear terms can include

$$u^2, uu_t, u_t^2, uu_{xx}, (u_x)^2, uu_{txx}, u_t u_{xx}, u_x u_{tx}, \tag{3.1}$$

while cubic nonlinearities can include terms such as

$$u^3, uu_t^2, u^2 u_t, u_t^3, (uu_{xx})u_t, (u_x)^2 u_t, u^2 u_{txx}, uu_t u_{xx}, uu_x u_{tx}\,. \tag{3.2}$$

Similar terms (without the u_t contributions) have been incorporated into various generalization of the Swift–Hohenberg equation (Burke & Dawes, 2012; Crawford & Riecke, 1999; Kozyreff & Tlidi, 2007). Including all the nonlinearities mentioned would make the model very complicated. We consider the two criteria identified at the beginning of this section and proceed to create a candidate nonlinear model of the form,

$$\frac{\partial^2 u}{\partial t^2} = \mathscr{M}_1 u + \mathscr{M}_2 u_t + Q_1 u^2 + C_1 u^3 + C_2 u^2 u_t + C_3 u_t^3 . \tag{3.3}$$

In this model we have chosen simple polynomial nonlinearities in the form of u^2, u^3 and u_t^3 along with the additional mixed nonlinear term $u^2 u_t$, each with a constant coefficient.

The first step is to ensure global stability during evolution. In order to test this, we look to determine a Lyapunov function for the dynamics in the spirit of the Swift–Hohenberg equation. With this in mind, we consider the Lyapunov functional

$$\mathscr{F}(t) = \int_0^L \left[\frac{1}{2} u_t^2 - \frac{1}{2}\mu u^2 + \frac{1}{2}\left[\left(1 + \frac{\partial^2}{\partial x^2}\right) u\right]^2 - \frac{1}{3} Q_1 u^3 - \frac{1}{4} C_1 u^4 \right] \mathrm{d}x. \tag{3.4}$$

In the rest of this work, we consider a domain of length L with periodic boundary conditions. Our aim is to show that this function is bounded below and decreases with time for large u and u_t. Having $C_1 < 0$ is sufficient for $\mathscr{F}(t)$ to be bounded from below. Differentiating $\mathscr{F}(t)$ with respect to time we have

$$\frac{d\mathscr{F}}{dt} = \int_0^L \left[u_{tt} - \mu u + \left(1 + \frac{\partial^2}{\partial x^2}\right)^2 u - Q_1 u^2 - C_1 u^3 \right] u_t \, \mathrm{d}x \tag{3.5}$$

$$= \int_0^L \left[\nu u_t - b\left(1 + \frac{\partial^2}{\partial x^2}\right)^2 u_t + C_2 u^2 u_t + C_3 u_t^3 \right] u_t \, \mathrm{d}x. \tag{3.6}$$

If $u_t = 0$ for all x, then we see that the above relation vanishes with $d\mathscr{F}/dt = 0$ and we have an equilibrium. Now, we consider a non-equilibrium point in the dynamics with large non-zero values of u and u_t and want show that the rate of change of $\mathscr{F}$ is still negative. In order to do this, we can simplify the expression above a bit further. At large u and u_t, the last two quartic terms dominate, so we write them as follows:

$$T = \int_0^L \left[C_2 u^2 u_t^2 + C_3 u_t^4 \right] \mathrm{d}x. \tag{3.7}$$

We can re-cast the states into an amplitude-phase form with

$$u(x,t) = R\cos\varphi, \qquad \text{and} \qquad u_t(x,t) = R\sin\varphi, \tag{3.8}$$

where $R(x,t)$ is a large radius and $\phi(x,t)$ is an angle. Substituting (3.8) into (3.7) and simplifying, we get

$$T = \int_0^L \left[R^4 \left(\frac{1}{2}\left(C_2 + C_3\right) + \frac{1}{2}\left(C_2 - C_3\right)\cos 2\varphi \right) \sin^2\varphi \right] \mathrm{d}x. \tag{3.9}$$

If trajectories are to remain bounded for any choice of ν, $d\mathscr{F}/dt$ must be negative for any (u, u_t) large enough as long as u_t is not zero for all x. This is guaranteed if $T < 0$ for any φ as long as $\sin\varphi$ is not zero for all x, which requires

$$C_2 + C_3 < 0 \qquad \text{and} \qquad 0 < \sqrt{\left(\frac{1}{2}\left(C_2 - C_3\right)\right)^2} < -\frac{1}{2}\left(C_2 + C_3\right) \implies C_2 C_3 > 0\,. \tag{3.10}$$

Therefore, the model second-order partial differential equation takes the following form

$$\frac{\partial^2 u}{\partial t^2} = \left(\mu - \left(1 + \frac{\partial^2}{\partial x^2}\right)^2\right)u + \left(\nu - b\left(1 + \frac{\partial^2}{\partial x^2}\right)^2\right)\frac{\partial u}{\partial t} + Q_1 u^2 + C_1 u^3 + C_2 u^2 u_t + C_3 u_t^3, \tag{3.11}$$

where μ and ν are the control parameters; $b > 1$, Q_1, C_1, C_2 and C_3 are constants coefficients with $C_1 < 0$ to make $\mathscr{F}$ bounded below; and we choose $C_2 < 0$ and $C_3 < 0$ to make $\mathscr{F}$ decrease with time at large values of u or u_t.

Now that we have identified conditions on the coefficients of the nonlinear terms in order to ensure global stability, we look at our second goal: to access all the possible dynamical behaviours close to a TB bifurcation. The process to check this in detail is discussed in Section 5. In order to increase the number of scenarios that are possible, we add one quadratic nonlinear term and two cubic nonlinear terms as shown below:

$$\frac{\partial^2 u}{\partial t^2} = \mathscr{M}_1 u + \mathscr{M}_2 u_t + Q_1 u^2 + C_1 u^3 + C_2 u^2 u_t + C_3 u_t^3 + Q_2 u u_{xx} + C_4 (u_x)^2 u_t + C_5 u u_x u_{tx}. \tag{3.12}$$

We do not calculate the Lyapunov functional for this updated model, but rather rely on the conditions that we have derived previously in terms of C_1, C_2 and C_3 to provide global stability and analyse this system in a domain of length L with periodic boundary conditions.

4. Reduction to the TB normal form

In this section, we use weakly nonlinear theory to reduce our model PDE from (3.12) to the TB normal form in (1.1). We consider $\epsilon \ll 1$ to be a small parameter that parameterizes the small amplitude solution such that $u = \mathscr{O}(\epsilon)$. This solution can be found in the neighbourhood of the TB bifurcation point where μ and ν vary with values of the order of $\mathscr{O}(\epsilon^2)$. This scaling satisfies both the normal forms of a pitchfork and a Hopf bifurcation and has been used to analyse the TB problem previously (Dangelmayr & Knobloch, 1987; Knobloch & Proctor, 1981). Therefore, we scale the field, time and the parameters μ and ν as follows:

$$u = \epsilon u_1 + \epsilon^2 u_2 + \epsilon^3 u_3 + \epsilon^4 u_4 + \cdots, \quad \frac{\partial}{\partial t} \to \epsilon \frac{\partial}{\partial t}, \quad \mu \to \epsilon^2 \mu_2, \quad \nu \to \epsilon^2 \nu_2. \tag{4.1}$$

By substituting the scalings into the governing equation (3.12), we get the following equation, where we write the terms up to $\mathcal{O}(\epsilon^4)$ explicitly.

$$\begin{aligned}\frac{\partial^2\left(\epsilon^3 u_1+\epsilon^4 u_2\right)}{\partial t^2} = {} & \mu_2\left(\epsilon^3 u_1+\epsilon^4 u_2\right)-\left(1+\frac{\partial^2}{\partial x^2}\right)^2\left(\epsilon u_1+\epsilon^2 u_2+\epsilon^3 u_3+\epsilon^4 u_4\right)\\ & +\nu_2\left(\epsilon^4\frac{\partial u_1}{\partial t}\right)-b\left(1+\frac{\partial^2}{\partial x^2}\right)^2\left(\epsilon^2\frac{\partial u_1}{\partial t}+\epsilon^3\frac{\partial u_2}{\partial t}+\epsilon^4\frac{\partial u_3}{\partial t}\right)\\ & +Q_1\left(\epsilon^2 u_1^2+2\epsilon^3 u_1 u_2+\epsilon^4 u_2^2+2\epsilon^4 u_1 u_3\right)\\ & +Q_2\left(\epsilon^2 u_1\frac{\partial^2 u_1}{\partial x^2}+\epsilon^3\left(u_1\frac{\partial^2 u_2}{\partial x^2}+u_2\frac{\partial^2 u_1}{\partial x^2}\right)+\epsilon^4\left(u_1\frac{\partial^2 u_3}{\partial x^2}+u_2\frac{\partial^2 u_2}{\partial x^2}+u_3\frac{\partial^2 u_1}{\partial x^2}\right)\right)\\ & +C_1\left(\epsilon^3 u_1^3+3\epsilon^4 u_1^2 u_2\right)+C_2\left(\epsilon^4 u_1^2\frac{\partial u_1}{\partial t}\right)+C_4\left(\epsilon^4 u_1\frac{\partial u_1}{\partial t}\frac{\partial^2 u_1}{\partial x^2}\right)\\ & +C_5\left(\epsilon^4 u_1\frac{\partial u_1}{\partial x}\frac{\partial^2 u_1}{\partial x\partial t}\right)+\mathcal{O}(\epsilon^5).\end{aligned} \tag{4.2}$$

Note that C_3 is not present in the above equation since it contributes only at the sixth order of ϵ. Matching terms of order ϵ and ϵ^2 we get

$$\mathcal{O}(\epsilon):\quad 0=\mathscr{L}u_1, \tag{4.3}$$

$$\mathcal{O}(\epsilon^2):\quad 0=\mathscr{L}u_2+b\mathscr{L}\frac{\partial u_1}{\partial t}+Q_1 u_1^2+Q_2 u_1\frac{\partial^2 u_1}{\partial x^2}, \tag{4.4}$$

where $\mathscr{L}$ is the linear operator defined as

$$\mathscr{L}=-\left(1+\frac{\partial^2}{\partial x^2}\right)^2. \tag{4.5}$$

The linear (4.3) obtained at $\mathcal{O}(\epsilon)$ can be solved for u_1 by assuming exponential solutions of the form

$$u_1(x,t)=F_1(t)e^{ix}+\bar{F}_1(t)e^{-ix}. \tag{4.6}$$

Here F_1 and its complex conjugate are functions of time. Substituting this and its derivatives into Eqn. (4.4), we can solve for u_2 as

$$u_2(x,t)=\frac{(Q_1-Q_2)}{9}F_1^2e^{2ix}+G_1e^{ix}+2(Q_1-Q_2)|F_1|^2+\bar{G}_1e^{-ix}+\frac{(Q_1-Q_2)}{9}\bar{F}_1{}^2e^{-2ix}, \tag{4.7}$$

where G_1 and $\bar{G}_1$ are functions of time.

At $\mathscr{O}(\epsilon^3)$, we have

$$\frac{\partial^2 u_1}{\partial t^2} = \mu_2 u_1 + \mathscr{L} u_3 + b\mathscr{L}\frac{\partial u_2}{\partial t} + 2Q_1 u_1 u_2 + Q_2\left(u_1\frac{\partial^2 u_2}{\partial x^2} + u_2\frac{\partial^2 u_1}{\partial x^2}\right) + C_1 u_1^3. \tag{4.8}$$

We can solve for u_3 by assuming it to be of the form

$$u_3(x,t) = H_3(t)e^{3ix} + H_2(t)e^{2ix} + H_1(t)e^{ix} + H_0(t) + \bar{H_1}(t)e^{-ix} + \bar{H_2}(t)e^{-2ix} + \bar{H_3}(t)e^{-3ix}, \tag{4.9}$$

Equation (4.8) has contributions into the e^{ix} lengthscale. However, this lengthscale has already been accounted for in the solution for u_1. Therefore, we need to enforce the condition that the coefficient of e^{ix} terms are zero as a solvability condition. Substituting (4.6), (4.7) and (4.9) into (4.8) and collecting the terms that contribute at the e^{ix} lengthscale, we get

$$\frac{\partial^2 F_1}{\partial t^2} = \mu_2 F_1 + A|F_1|^2 F_1, \tag{4.10}$$

where

$$A = \left(Q_1 - Q_2\right)\left(\frac{38}{9}Q_1 - \frac{23}{9}Q_2\right) + 3C_1. \tag{4.11}$$

We can then solve for the unknowns $H_{0,2,3}$ by collecting the coefficients of the constant, e^{2ix} and e^{3ix} respectively as

$$H_0 = 2\left(Q_1 - Q_2\right)\left(F_1\bar{G_1} + \bar{F_1}G_1 - b\left(\frac{\partial F_1}{\partial t}\bar{F_1} + F_1\frac{\partial \bar{F_1}}{\partial t}\right)\right). \tag{4.12}$$

$$H_2 = \frac{2\left(Q_1 - Q_2\right)}{9}\left(F_1 G_1 - bF_1\frac{\partial F_1}{\partial t}\right), \tag{4.13}$$

$$H_3 = \frac{1}{64}\left(\frac{2}{9}Q_1\left(Q_1 - Q_2\right) - \frac{5}{9}Q_2\left(Q_1 - Q_2\right) + C_1\right)F_1^3. \tag{4.14}$$

At $\mathscr{O}(\epsilon^4)$, we have

$$\begin{aligned}\frac{\partial^2 u_2}{\partial t^2} &= \mu_2 u_2 + \mathscr{L} u_4 + \nu_2\frac{\partial u_1}{\partial t} + b\mathscr{L}\frac{\partial u_3}{\partial t} + Q_1\left(u_2^2 + 2u_1 u_3\right)\\ &\quad + Q_2\left(u_1\frac{\partial^2 u_3}{\partial x^2} + u_2\frac{\partial^2 u_2}{\partial x^2} + u_3\frac{\partial^2 u_1}{\partial x^2}\right) + 3C_1 u_1^2 u_2 + C_2 u_1^2\frac{\partial u_1}{\partial t}\\ &\quad + C_4 u_1\frac{\partial u_1}{\partial t}\frac{\partial^2 u_1}{\partial x^2} + C_5 u_1\frac{\partial u_1}{\partial x}\frac{\partial^2 u_1}{\partial x \partial t}.\end{aligned} \tag{4.15}$$

The solvability condition from this order of equations is the e^{ix} component of (4.15):

$$\frac{\partial^2 G_1}{\partial t^2} = \mu_2 G_1 + \nu_2 \frac{\partial F_1}{\partial t} + N F_1^2 \bar{G}_1 + P|F_1|^2 G_1 + C\left(\frac{\partial F_1}{\partial t}\bar{F}_1 + F_1 \frac{\partial \bar{F}_1}{\partial t}\right) F_1 + D|F_1|^2 \frac{\partial F_1}{\partial t}, \tag{4.16}$$

where

$$N = (Q_1 - Q_2)\left(\frac{38}{9}Q_1 - \frac{23}{9}Q_2\right) + 3C_1, \tag{4.17}$$

$$P = (Q_1 - Q_2)\left(\frac{76}{9}Q_1 - \frac{62}{9}Q_2\right) + 6C_1, \tag{4.18}$$

$$C = 2b\,(Q_1 - Q_2)\,(-2Q_1 + Q_2) + C_2 - C_4 + C_5, \tag{4.19}$$

$$D = b\,(Q_1 - Q_2)\left(\frac{-4}{9}Q_1 + \frac{10}{9}Q_2\right) + C_2 + 3C_4 - C_5. \tag{4.20}$$

In order to ensure that both the solvability conditions arising from both the $\mathscr{O}(\epsilon^3)$ and $\mathscr{O}(\epsilon^4)$ equations are satisfied, we use a reconstitution procedure (Rucklidge & Silber, 2009) to combine (4.10) and (4.16) into a single PDE by defining a new variable

$$z = \epsilon F_1 + \epsilon^2 G_1. \tag{4.21}$$

By unscaling time and the parameters according to

$$\frac{\partial}{\partial t} \to \frac{1}{\epsilon}\frac{\partial}{\partial t} \qquad \mu_2 \to \frac{1}{\epsilon^2}\mu \qquad \text{and } \nu_2 \to \frac{1}{\epsilon^2}\nu. \tag{4.22}$$

We get

$$\begin{aligned}\frac{\partial^2 z}{\partial t^2} = \mu z + \epsilon\nu \frac{\partial F_1}{\partial t} + \epsilon^3 A|F_1|^2 F_1 + \epsilon^4 N F_1^2 \bar{G}_1 + \epsilon^4 P|F_1|^2 G_1 \\ + \epsilon^3 C\left(\frac{\partial F_1}{\partial t}\bar{F}_1 + F_1\frac{\partial \bar{F}_1}{\partial t}\right) F_1 + \epsilon^3 D|F_1|^2 \frac{\partial F_1}{\partial t}.\end{aligned} \tag{4.23}$$

Substituting $F_1 = \frac{z}{\epsilon} - \epsilon G_1$ in (4.23) and collecting terms of $\mathscr{O}(1)$ in the above equation, we get the TB normal form as

$$\frac{\partial^2 z}{\partial t^2} = \mu z + \nu\frac{\partial z}{\partial t} + A|z|^2 z + C\left(\frac{\partial z}{\partial t}\bar{z} + z\frac{\partial \bar{z}}{\partial t}\right) z + D|z|^2\frac{\partial z}{\partial t}, \tag{4.24}$$

where A, C and D are given by (4.11), (4.19) and (4.20), respectively.

5. Accessing possible different dynamical behaviour near the TB bifurcation

In this section, we identify parameter combinations in the model at which we can observe different dynamical behaviours close to the TB bifurcation. In order to do this, we relate the parameters in the current model with those investigated in detail by Dangelmayr & Knobloch (1987). In the rest of this paper, we refer to this paper as DK. DK identify different bifurcation scenarios close to a TB bifurcation and classify them in terms of the value of coefficient A as well as the ratio $D/(2C+D)$ where $2C+D$ is defined as M. The ratio can be related to the coefficients in our model as below:

$$\frac{D}{M} = \frac{-4bQ_1^2 + 14bQ_1Q_2 - 10bQ_2^2 + 9C_2 + 27C_4 - 9C_5}{-76bQ_1^2 + 122bQ_1Q_2 - 46bQ_2^2 + 27C_2 + 9C_4 + 9C_5}. \tag{5.1}$$

We consider a few special cases below to illustrate the need for certain nonlinear terms in the model. First, let us consider the case with $Q_2 = C_4 = C_5 = 0$. Then using expressions in (4.11) and (4.20), the values of A and D will be negative and the fraction D/M is always bounded between the values

$$\frac{1}{19} < \frac{D}{M} < \frac{1}{3}.$$

In this range of ratios, we can only access one type of bifurcation behaviour near the TB bifurcation identified from the classification given in DK as $A < 0$, case II $-$.

Secondly, we consider the case with only $C_4 = C_5 = 0$, which gives the expression for the ratio D/M as

$$\frac{D}{M} = \frac{-4bQ_1^2 + 14bQ_1Q_2 - 10bQ_2^2 + 9C_2}{-76bQ_1^2 + 122bQ_1Q_2 - 46bQ_2^2 + 27C_2}, \tag{5.2}$$

Considering that Lyapunov stability requires C_1, C_2 and C_3 to be negative, we consider the case with $C_1 = C_2 = C_3 = -1$ and $b = 2$. By plotting contours of A and $\frac{D}{M} = c$, where $c = \frac{1}{5}, \frac{1}{2}, 0.7, 0.74, \frac{3}{4}, \frac{4}{5}, 1$, we can obtain a range of normal form cases. Figure 3 shows the regions of different cases accessible in this case as a function of the two quadratic coefficients Q_1 and Q_2. From this figure, we see that we can access all bifurcation scenarios with $A < 0$, while in the case with $A > 0$, we are unable to access cases I $-$ and IV $-$. For other choices of parameters, it is possible to access all cases on the normal form with $M < 0$, while still satisfying the Lyapunov stability requirement. However, cases of the normal form with $M > 0$ still remain inaccessible with $C_4 = C_5 = 0$.

Thirdly, when we allow for all nonlinear terms in the model, we can access all cases of the normal form listed in DK, i.e. 18 cases with $A < 0$ and 8 cases with $A > 0$ both with $M < 0$ and $M > 0$. As a first reference, we give a list of parameters that allow us to reach all the cases with $M < 0$ in Table 2. Each of these cases has a different bifurcation scenario close to the TB bifurcation.

Of all these cases, we choose two to look at in detail. Our choice is guided by the predicted stability diagrams from DK, which indicate the possibility of interesting coexistence regions of different states, e.g., coexistence of the trivial and a patterned SS, coexistence of SS and SW, etc. Cases of particular interest are IV- with $A > 0$ and I- with $A < 0$ in DK and marked in blue in Table 2.

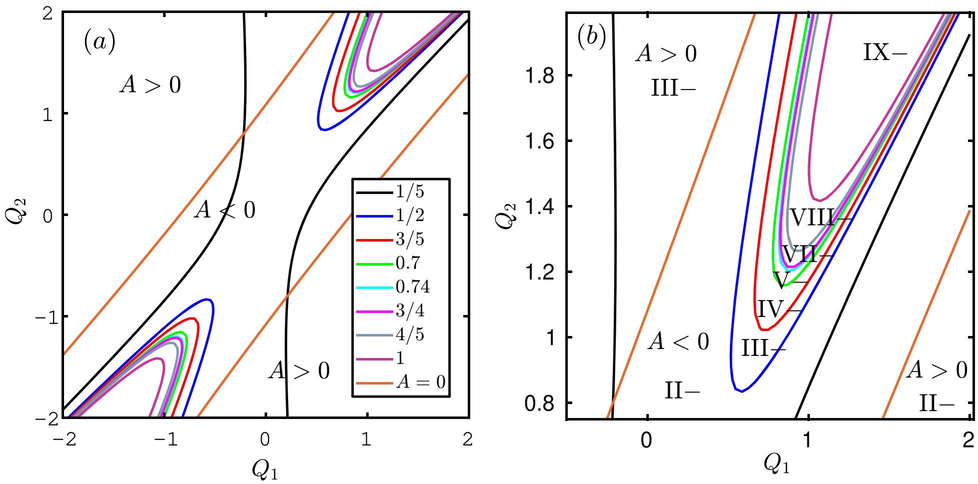

FIG. 3. (*a*) Plot of the contours of $A = 0$ in orange from (4.11) and the different values of $\frac{D}{M} = c$ where $c = \frac{1}{5}, \frac{1}{2}, \frac{3}{5}, 0.7, 0.74, \frac{3}{4}, \frac{4}{5}$ from (5.2) where $C_1 = C_2 = C_3 = -1$ and $b = 2$. The regions between each curve correspond to the enumerated II −,... IX − cases in DK. (*b*) Zoomed in view of the top right corner of (*a*).

TABLE 2 *Examples of parameter values in the model (3.12) to access different cases in the normal form in DK. Only cases with $M < 0$ are listed here. The instances in blue indicate the cases we considered in this paper with the main result*

Case in DK	Coefficients of the nonlinearities Q_1	Q_2	C_1	C_2	C_3	C_4	C_5
$A > 0$							
I −	0.8	−0.5	−1	−0.1	−1	−0.1	−5
II −	1.5	0.5	−1	−1	−1	0	0
III −	0.1	1.5	−1	−1	−1	0	0
IV −	0.9	−0.2	−0.2	−1	−1	−0.5	6
$A < 0$							
I −	0.8	0.5	−1	−0.1	−1	−0.1	−5
II −	0.5	0	−1	−1	−1	0	0
III −	0.6	0.9	−1	−1	−1	0	0
IV −	0.8	1.1	−1	−1	−1	0	0
V −	0.85	1.2	−1	−1	−1	0	0
VI −	0.9	1.21	−1	−1	−1	0	0
VII −	0.9	1.25	−1	−1	−1	0	0
VIII −	1	1.4	−1	−1	−1	0	0
IX −	1.1	1.5	−1	−1	−1	0	0

6. Localized SS

The first case that we discuss is the one labelled as case *IV* with $A > 0$ in DK. Figure 4(*a*) shows the stability in (ν, μ)-plane as predicted by the TB normal form in DK. Here we observe that there is a small unstable branch of SS that lies in the third quadrant (where the TS is stable). Further, we observe a stable

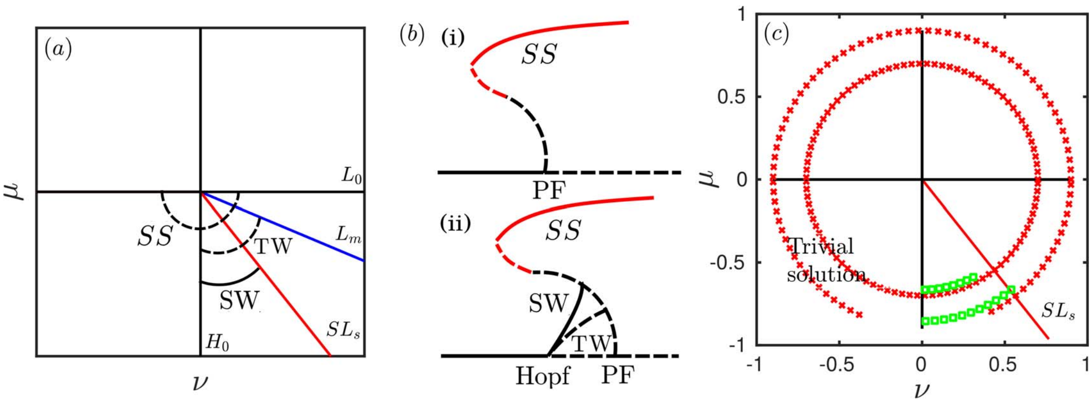

FIG. 4. (*a*) Sketch of the stability diagram for case IV with $A > 0$ in (ν, μ)-plane and (*b*) the corresponding bifurcation diagram from (Dangelmayr & Knobloch, 1987), where the panel (i) represents the bifurcation above the diagonal ($\nu = \mu$) in the (ν, μ)-plane and the panel (ii) represents the bifurcation below the diagonal ($\nu = \mu$) in the (ν, μ)-plane. In this bifurcation diagrams, the black lines (solid for stable solutions, dashed for unstable solutions) are from DK, while the red lines are inferred from our system given Lyapunov stability. (*c*) Plot of the solution from solving the model (3.12) by time stepping with parameters values $Q_1 = 0.9, Q_2 = -0.2, C_1 = -0.2, C_2 = C_3 = -1, C_4 = -0.5, C_5 = 6$ and $b = 2$ for radius $r = 0.7, 0.9$. A Hopf bifurcation occurs at $\theta = 270°$ and a pitchfork bifurcation occurs at $\theta = 180°$ and $\theta = 0°$. The red x and green square refer to extended SS and SW solutions, respectively. The half line SL_s is the line of heteroclinic bifurcations where SW joins the small-amplitude unstable SS.

branch of SW in the fourth quadrant along with the unstable branch of SS. We identify this bifurcation scenario to be interesting as we expect the possibility for localized steady states in a background of trivial state (LSS-TS) in the third quadrant and the possibility for LSS in a background of standing waves (LSS-SW) in the fourth quadrant.

Figure 4(*b*) shows the predicted bifurcation diagrams (in black lines) from the TB normal form equation. The two cases correspond to the cases of variation of parameters along the diagonal above and below the line $\mu = \nu$ respectively. The bifurcation above the diagonal in (ν, μ)-plane (see Fig. 4(*b*)(i)) has only a subcritical SS branch from a pitchfork bifurcation at $\mu = 0$. The TS is stable in the region where $\mu < 0$ and $\nu < 0$. The bifurcation below the diagonal in (ν, μ)-plane (see Fig. 4(*b*), right panel) has a subcritical SS branch from a pitchfork bifurcation at $\mu = 0$. Stable SW and unstable TW bifurcate from the TS at a Hopf bifurcation where $\nu = 0, \mu < 0$. The stable SW branch terminates on the subcritical SS branch with the formation of a heteroclinic orbit at a global bifurcation SL_s connecting two saddles (the notation for these bifurcations follows DK). The unstable TW branch terminates at the subcritical SS at L_m. This scenario has been investigated analytically and numerically in thermosolutal convection (Da Costa *et al.*, 1981; Huppert & Moore, 1976; Knobloch *et al.*, 1986; Knobloch & Proctor, 1981) and is important because it was an early example of the discovery and analysis of how a Shil'nikov heteroclinic orbit (Knobloch *et al.*, 1986) can lead to chaotic dynamics, though this is in a different parameter regime from that which we will investigate. To the bifurcation diagrams in Fig. 4(*b*), we add predictions (from global stability requirements) of a large amplitude stable branch of steady patterned state (in red lines). This figure now illustrates the possible coexistence regions that could allow for the localized states detailed in the previous paragraph.

In order to confirm the existence of a stable large amplitude branch of patterned state (SS), we first look at asymptotic states accessible via time stepping. We treat the model numerically by discretizing the PDE both in time and space. In space, we discretize the model using spectral methods (Canuto *et al.*, 2012; Hussaini & Zang, 1987) and fast Fourier transform with 16 grid points per wavelength. In time, we discretize the model using the exponential time differencing (ETD) method (Cox & Matthews, 2002; Kassam & Trefethen, 2005). The ETD method solves the linear parts of the PDEs exactly followed by a second-order approximation of the nonlinear parts. We compare the stability region from solving the model with the stability region obtained from the normal form (Dangelmayr & Knobloch, 1987). To do this we solve the PDE and plot the type of solutions in (ν, μ)-plane, using polar coordinates defined as

$$\nu = r\cos(\theta), \qquad \mu = r\sin(\theta), \tag{6.1}$$

where r is the radius that controls how far ν and μ are from the TB point, and θ is the angle that controls the position of ν and μ in the (ν, μ)-plane. Note that the Hopf bifurcation occurs at $\nu = 0$ and $\mu < 0$ which correspond to $\theta = 270°$. The pitchfork bifurcation occurs at $\mu = 0$ which correspond to $\theta = 0°$ and $\theta = 180°$.

Figure 4(c) shows the results of starting time stepping from different initial conditions for a variety of system parameters at two different radii $r = 0.7$ and $r = 0.9$. At radius $r = 0.7$, we start from initial conditions close to a pitchfork bifurcation at $\theta = 180°$. We are able to obtain large amplitude SS solutions (shown as red crosses) as well as recover the TS (not shown with markers). The TS is stable when $\mu < 0$ and $\nu < 0$ until we reach a Hopf bifurcation close to $\theta = 270°$. At this bifurcation, the TS loses stability and a new branch of SW are created (shown as green crosses). The amplitude of the SW branch increases with increasing $270° < \theta < 297°$, which is close to the prediction of an SL_s bifurcation at an angle of $\theta = 308°$ from the normal form analysis. The complete circle of red crosses observed for the large amplitude SS in Fig. 4(c) at $r = 0.7$ indicates that the solution branch of large amplitude SS is disconnected from the low amplitude SS solution branch when viewed as a function of θ.

At a slightly larger radius with $r = 0.9$, time stepping identifies similar coexistence of TS and large amplitude SS solutions in the third quadrant. However, the large amplitude SS solutions exist only until $\theta = 245°$. At $\theta = 270°$, we encounter the Hopf bifurcation, as before, resulting in the branch of SW solutions. The branch of SW exists in the range of $270° < \theta < 309°$ and terminate close to the prediction of the SL_s bifurcation. We find that we are able to recover the large amplitude SS branch again from $\theta = 297°$. The fact that we are able to identify two θ values where the large amplitude SS solution branch terminates indicates that they are the locations of saddle-node bifurcations where the large amplitude SS branch connects with the low amplitude SS branch.

Figure 4(c) has identified two bistable regions: bistability between the TS and large-amplitude SS when $\mu < 0$, $\nu < 0$ and bistability between small-amplitude SW and large-amplitude SS in the region between $\nu = 0$, $\mu < 0$ and the half line SL_s. We now look to obtain localized states in these regions. To do this we follow the process. First, we increase the domain size to allow 64 wavelengths and perform time stepping to find an extended SS. Then, we use a sech-envelope with different widths to construct several initial conditions and perform time stepping again to obtain nearby dynamically stable localized states. Using this method we are able to get LSSs, LSS in both of the bistable regions with two different backgrounds.

First, we find LSS-TS, which has a localized steady state with a trivial state as a background in the region where the TS and large-amplitude SS are both stable ($\mu < 0$ and $\nu < 0$). Figure 5(a) shows one example of LSS with TS background for radius 0.7 and $\theta = 200°$ ($\nu = -0.54$, $\mu = -0.45$). There are other LSS-TS with different widths, depending on the initial conditions, and to investigate these in detail we perform numerical continuation in the next section.

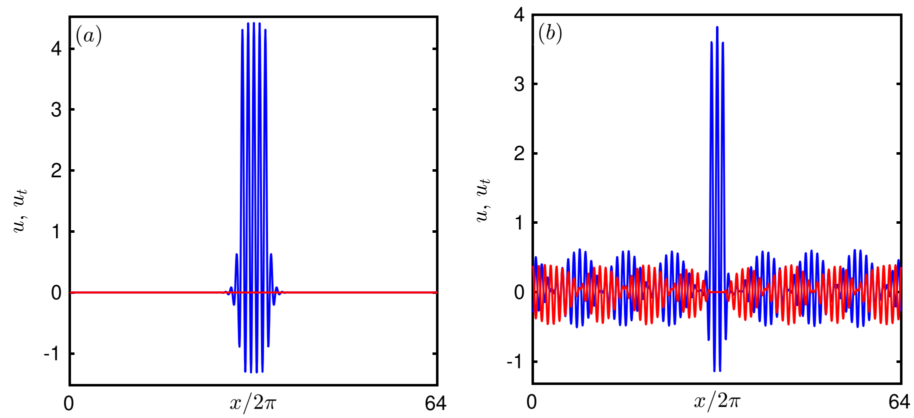

FIG. 5. (*a*) LSS with trivial solutions background from time stepping at radius 0.7 and $\theta = 220°$ where $\nu = -0.54, \mu = -0.45$. (*b*) LSS with MW solutions background from time stepping at radius 0.7 and $\theta = 280°$ where $\nu = 0.12, \mu = -0.69$. The blue and red curves refer to u and u_t, respectively. A movie of the state in (*b*) is available at (Alrihieli *et al.*, 2020).

Second, we find LSS with an MW background in the region where the large-amplitude SS and the small-amplitude SW are both stable. The bistability occurs in the region between the Hopf bifurcation at $\theta = 270°$ ($\nu = 0, \mu < 0$) to the half line SL_s at $\theta \approx 308.4°$, as mentioned above. The small-amplitude MW background solutions move as a function of time. Initially, the small-amplitude solutions are SW with large-amplitude SS in the middle of the domain. As time increases the SW turn in to MW. This change occurs because the left-right symmetry of the SW solutions is broken by the SS solutions in the middle. Figure 5(*b*) shows one example of LSS with MW background for radius 0.7 and $\theta = 280°$ ($\nu = 0.12, \mu = -0.69$). Many widths of this class of solutions can be obtained by altering the initial width of the sech-envelope.

Unlike the LSS-TS, in this case two patterns (large-amplitude SS and small-amplitude MW) coexist, which suggests the presence of a spatial heteroclinic orbit between the SS and MW states (cf. Beck *et al.* (2009)).

6.1 *Numerical continuation*

In the following we use numerical continuation to compute steady numerical solutions of the model for both the extended SS and the LSS. The method we use is based on Newton iteration and pseudo arclength continuation (Doedel *et al.*, 1991). Seting the time-derivative terms to zero in (3.12) results in the steady Swift–Hohenberg equation:

$$0 = \left(\mu - \left(1 + \frac{\partial^2}{\partial x^2}\right)^2\right)u + Q_1u^2 + Q_2uu_{xx} + C_1u^3. \tag{6.2}$$

We note that even when the solutions depend only on μ, the stability depends on both μ and ν. The initial guesses for the branches of extended SS and LSS are obtained from time stepping. Since θ controls the values of μ and ν in the (ν, μ)-plane, we will use θ as the bifurcation parameter with fixed radius. We show the bifurcation diagram of all solutions as functions of θ and μ, where $\mu = r\sin(\theta)$, against the

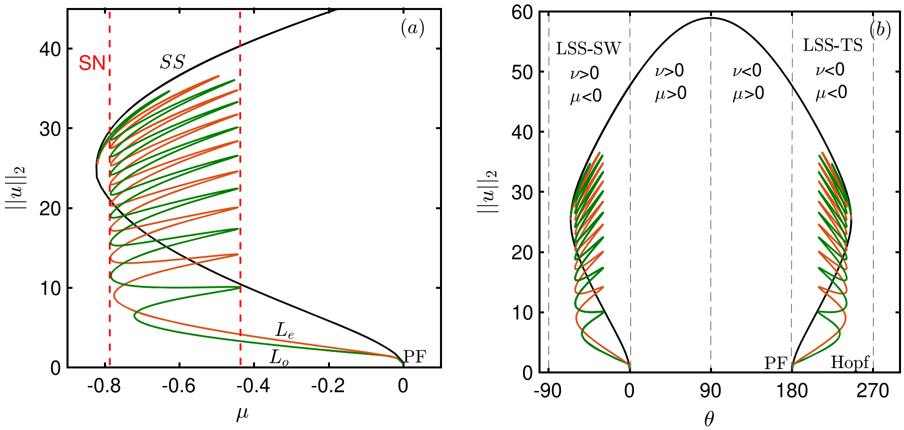

FIG. 6. The full branch for extended SS in black and the odd L_0 and even L_e localized SS branches in green and brown where (*a*) μ is the control parameter and (*b*) θ is the control parameter, both for the case with radius $r = 0.9$.

norm as a measure of the solutions, where

$$||u||_2 = \int_0^L (u(x))^2 \mathrm{d}x. \tag{6.3}$$

We will perform continuation at two different radii $r = 0.7$ and $r = 0.9$ in a 1D domain allowing 16 wavelengths with 16 grid points per wavelength.

6.1.1 *Continuation for radius 0.9.* Starting from initial guesses obtained from time stepping in numerical continuation with radius $r = 0.9$, we perform continuation to obtain the extended SS and the LSS-TS solutions. Figure 6 shows the solutions from numerical continuation with $\mu = r \sin\theta$ as the control parameter in panel (*a*) and with θ as the control parameter in panel (*b*) for radius $r = 0.9$. In Fig. 6(*a*), we represent the full branch of extended SS in black, the LSS branch with even numbers of peaks L_e in orange and the LSS branch with odd numbers of peaks L_o in green. Along the odd branch L_o the midpoint ($x = Lx/2$) of the localized state is always a global maximum (with an odd number of maxima), while along the even branch L_e the midpoint ($x = Lx/2$) is a global minimum (with an even number of maxima). The extended SS branch emerges subcritically from the TS at the pitchfork bifurcation $\mu = 0$ ($\theta = 180°$) and undergoes a saddle-node bifurcation at $\mu = -0.81$ ($\theta = 245.6°$). The branch changes at the saddle-node to a large-amplitude stable state. The picture in panel (*a*) of the extended SS branch along with the LSS-TS branches is exactly what we see in the Swift-Hohenberg equation (given that 3.12 reduces to a Swift–Hohenberg equation at equilibria with vanishing u_t, such as SSs). An example of a state with a LSS in a TS background is shown in Fig. 5(*a*).
In the co-dimension 2 view obtained in Fig. 6(*b*) with θ as the bifurcation parameter, the results discussed above form the snaking structure seen between the range $180° < \theta < 250°$. We observe that for further changes of θ to values less than 180°, the branch of extended SSs increases in magnitude and reaches the maximum amplitude when $\theta = 90°$ and decreases until reaches to the second saddle-node at $\theta = -65.6°$. The branch then decrease further until terminates back to a pitchfork bifurcation $\theta = 0°$. Given that the TS is stable only when both $\mu < 0$ and $\nu < 0$, TS is unstable in the range

$270^\circ < \theta < 180^\circ$, by undergoing a Hopf bifurcation at $\theta = 270^\circ$. After the Hopf bifurcation, LSS-TS exist, but the stable solutions are the LSS with an MW background where there is bistability between SS and SW. An example of such a LSS-MW state is shown in Fig. 5(*b*).

Figure 7 summarizes the results obtained from numerical continuation at different radii in the (ν, μ)-plane for two chosen radii $r = 0.9$ and $r = 0.7$. The black curve refers to the extended SS and the blue curve refers to the region where LSS with the TS background exist. The region between the red dashed lines identifies the snaking region. In Fig. 7 we also show points obtained from time stepping where the LSS with an MW background exist as green stars. The SL_s half line is the line where the branch ends on a heteroclinic bifurcation (see Fig. 4). Beyond this line, there are no SW, and time stepping evolves to a large-amplitude SS.

7. Localized TW

The second case we discuss is the one labelled as case I with $A < 0$ in DK where $D > 0$ and $M < 0$. Figure 8(*a*) shows the prediction of different bifurcations and stable solutions from the TB normal form in DK. The normal form shows a stable SS occurring in the region between the pitchfork bifurcation at $\mu = 0$ with $\nu < 0$ and the half line L_m, where

$$L_m : \mu D = \nu A \qquad A\mu < 0. \tag{7.1}$$

The TW branch bifurcates subcritically from the trivial solution at the Hopf bifurcation at $\nu = 0$ with $\mu < 0$. Coupling this prediction from the normal form along with the global stability requirements of the model, we expect two different localized solutions in this case: a localized travelling wave in a background of the trivial state (LTW-TS) in the third quadrant, along with the possibility of a localized travelling wave in a background of the steady state (LTW-SS) in the second quadrant.

We consider two bifurcation scenarios to illustrate these cases, one above and one below the line $\mu = \nu$ and plot them in Fig. 8(*b*). The bifurcation below the diagonal in (ν, μ)-plane (see Fig. 8(*b*)(ii)) has an unstable SS branch bifurcating from a pitchfork bifurcation at $\mu = 0$ with $\nu > 0$. It also has a subcritical TW branch and unstable SW branch bifurcating from the TS at a Hopf bifurcation where $\nu = 0, \mu < 0$. The SW branch undergoes saddle-node (SN) bifurcation at SN_{s2} and terminates at the SS branch at L_M. From global stability, we expect the unstable branch of TW to regain stability at a saddle-node bifurcation, giving rise to a large amplitude branch of TW solutions (as shown by red lines in Fig. 8(*b*). The bifurcation above the diagonal in (ν, μ)-plane (see Fig. 8(*b*)(i)) has stable SS branch bifurcating from a pitchfork bifurcation at $\mu = 0$ with $\nu > 0$ which becomes unstable after passing the half lines L_m. The subcritical TW branch bifurcates from the SS branch at L_m. The TS is stable in the region where $\mu < 0$ and $\nu < 0$. This implies that we can expect coexistence between the large amplitude TW and the TS for values before the pitchfork bifurcation and we can expect coexistence between large amplitude TW and stable SS solutions in the range of values past the pitchfork bifurcation.

In order to explore the fully nonlinear behaviour of the system, we run timestepping from different initial conditions for a variety of parameters at three different radii $r = 0.1, 0.7, 0.9$ in a small (one wavelength) domain and plot the results in Fig. 8(*c*). In these calculations, we use 32 grid points per wavelength.

The TS is stable for the region $\nu < 0$ and $\mu < 0$ for all radii $r = 0.1, 0.7, 0.9$. The small-amplitude SS bifurcate at a pitchfork bifurcation $\theta = 180^\circ$ where $\mu = 0, \nu < 0$ and loses stability at L_m, which has the slope $\frac{\mu}{\nu} \approx -0.502$. There is a large-amplitude TW solution around the whole circle in the (ν, μ)-plane at radius $r = 0.1$. At radii $r = 0.7$ and $r = 0.9$, the amplitude of the TW decreases in the region

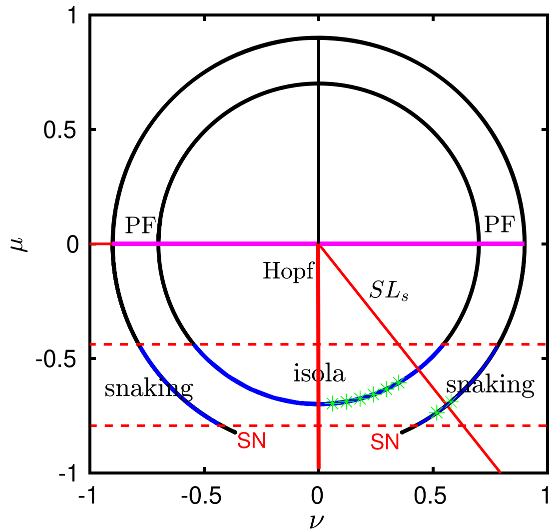

FIG. 7. (ν, μ)-plane from solving the PDE using numerical continuation for radii $r = 0.9$ and $r = 0.7$. The pink and red lines refer to the pitchfork bifurcation and Hopf bifurcation, respectively. The black curve refers to the extended SS solutions and the blue curve refers to the snaking regions. At $r = 0.9$, this homoclinic snaking occurs between $\mu = -0.44$ and $\mu = -0.78$. Red dashed lines mark the snaking region as shown previously in Fig. 6(a). The SN point of the extended SS solutions occurs at $\mu = -0.81$. The localized solutions stable in the region where the TSs is stable ($\mu < 0$ and $\nu < 0$) and unstable in the region where the TS is unstable ($\mu < 0$ and $\nu > 0$). The green star markers refer to the LSS with an MW background and are obtained from time stepping. The SL_s half line is the line where the bifurcation changes from SW to SS in the normal form (see Fig. 4).

where the TS or the small-amplitude SS are stable and we lose the branch solutions (at potential saddle-node bifurcations). This confirms that the fully nonlinear behaviour in this case allows for bistability between two different states: a large-amplitude TW with TSs in the region where $\mu < 0, \nu < 0$ and a large-amplitude TW with small-amplitude SS in the region between the pitchfork bifurcation $\mu = 0, \nu < 0$ to the half line L_m. Therefore, the LTW-TS and LTW-SS can be sought.

In order to obtain the localized state we increase the domain size to allow 64 wavelengths in the domain and perform time stepping to find an extended TW. To obtain the localized state, we use a sech-envelope with different widths and do time stepping to obtain the localized state. Using this method we are able to get LTW with two different backgrounds as shown in Figs 9 and 10.

First, we find LTW-TS in the region where $\mu < 0$ and $\nu < 0$. Figure 9 shows two examples of LTW with the TS background for two different parameters values (a) for radius $r = 0.1$ and $\theta = 200°$ where $\mu = -0.034, \nu = -0.094$ and (b) for radius $r = 0.1$ and $\theta = 250°$ where $\mu = -0.094, \nu = -0.034$. In these examples, the patterns of u and u_t move from left to right with a group velocity smaller than the phase velocity. At a given set of parameter values, the LTW we find all have the same width and move at a unique velocity, regardless of initial conditions. Starting simulations from a wide variety of initial conditions only ever evolves to either fully extended states (of the background pattern or a large amplitude TW) or a localized state with a unique width and velocity. So, unlike a LSS-TS or LSS-SW localization scenario, both the width and the velocity are unique at a given parameter set.

Second, we find LTW-SS in the region between the pitchfork bifurcation at $\mu = 0$ where $\nu < 0$ to the half line L_m. Figure 10 shows two examples of LTW with an SS background for (a) radius $r = 0.1$ and $\theta = 170°$ where $\mu = 0.017, \nu = -0.098$ and (b) for radius $r = 0.4$ and $\theta = 160°$ where

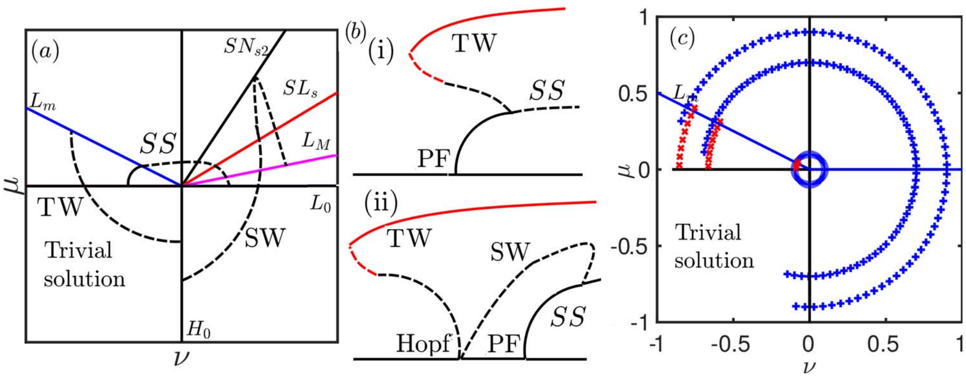

FIG. 8. (*a*) Sketch of the stability diagram for case I- with $A < 0$ in (ν, μ)-plane and (*b*) the corresponding bifurcation diagram from DK, where the panel (*b*)(i) represents the bifurcation above the diagonal in the (ν, μ)-plane and (*b*)(ii) represents the bifurcation below the diagonal in the (ν, μ)-plane. (*c*) Plot of solutions obtained through time stepping (3.12) with parameters values $Q_1 = 0.8, Q_2 = 0.5, C_1 = -1, C_2 = -0.1, C_3 = -1, C_4 = -0.1, C_5 = -5$ and $b = 2$ for radius 0.1, 0.7 and 0.9. A Hopf bifurcation occurs at $\theta = 270°$ and a pitchfork bifurcation occurs at $\theta = 180°$ and $\theta = 0°$. The blue + and red × refer to stable extended TW and SS solutions, respectively. The half line L_m is the line from the normal form at which the bifurcation from TW to SS occurs, at $\theta \approx 153.3°$.

$\mu = 0.14, \nu = -0.038$. The LTW move from left to right. Again, we find only LTW-SS with one chosen width and a corresponding unique velocity in this case. In both cases, changes in a system parameter cause only small changes to both the width and velocity of the LTW-SS.

In all these LTW examples, we started with initial conditions with a wide variety of widths, but always found a localized solution with the same width, unlike in the LSS cases.

8. Conclusions

In this paper, we have developed a simple nonlinear pattern-forming PDE model that has a TB primary bifurcation. The model is based on the Swift–Hohenberg equation, which was originally derived to describe the effects of thermal fluctuations and the evolution of roll patterns close to the onset of Rayleigh–Bénard convection and later used as a model of pattern formation in many physical problems. The new model can be reduced further using weakly nonlinear theory to the TB normal form where there are double zero eigenvalues, with an algebraic multiplicity of two and geometric multiplicity of one. The advantage of the model lies in the relative ease of investigating the nonlinear behaviour numerically and analytically, as compared to the full PDEs of double-diffusive convection. Alongside the numerical results, the model is important for helping to understand the bifurcation structure and the solution behaviour close the TB point in an extended system and in particular for investigating localized solutions.

We identified two types of localized states, which have previously been observed in various systems. The first of these is the LSS-TS, which was observed numerically in binary convection (Batiste *et al.*, 2006; Mercader *et al.*, 2009) and in thermosolutal convection (Beaume *et al.*, 2011). The second localized state is that of an LTW-TS, which was observed in binary convection (Barten *et al.*, 1991, 1995b; Jung & Lücke, 2005; Kolodner, 1991a,b,c; Niemela *et al.*, 1990; Surko *et al.*, 1991; Watanabe *et al.*, 2012; Zhao & Tian, 2015). We have further identified two new spatially localized states: that of a localized steady state in a modulated wave background (LSS-MW) and that of an LTW-SS.

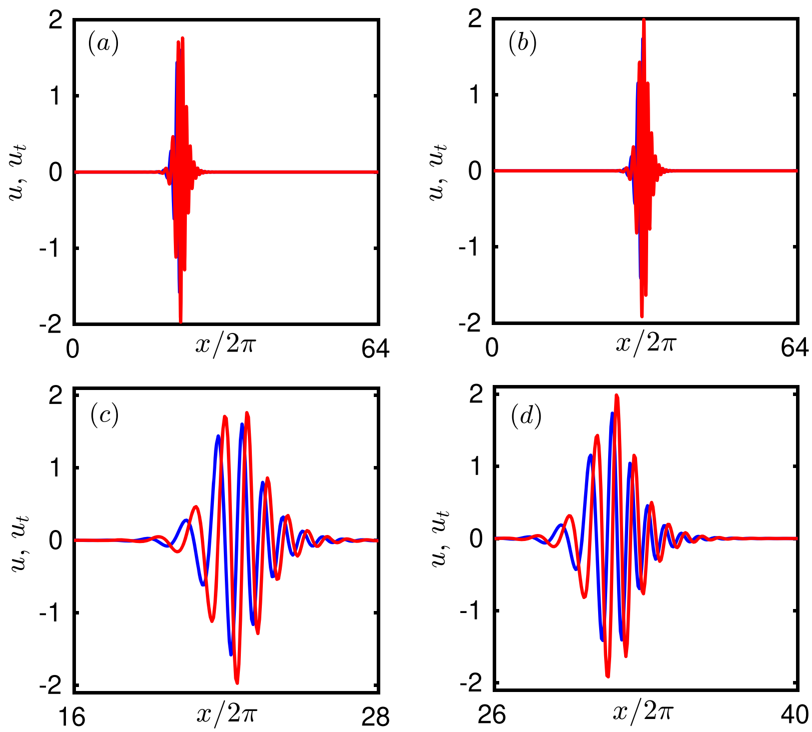

FIG. 9. Two examples of LTW with TS background. (*a*) For radius $r = 0.1$ and $\theta = 200^\circ$ and (*b*) radius $r = 0.1$ and $\theta = 250^\circ$. (*c*,*d*) Zooms of (*a*,*b*). The blue and red curves refer to u and u_t, and the waves travel to the right. A movie of the state in (*a*) is available at Alrihieli *et al.* (2020).

To find localized states, we looked for subcritical pitchfork and Hopf bifurcations, since we expected that subsequent saddle-node bifurcations would lead to stable large-amplitude solutions coexisting with the stable trivial solutions, and possibly then to localized solutions. We identified a subcritical pitchfork bifurcation for the case IV $-$ with $A > 0$ (see Fig. 4) and a subcritical Hopf bifurcation for the case I $-$ with $A < 0$ (see Fig. 8). From solving the model numerically, we obtained different types of localized states. In case IV $-$ with $A > 0$, we obtained LSS in the region where there is bistability between the TS and a branch of periodic SSs, with $\mu < 0$ and $\nu < 0$. We used numerical continuation of the PDE model (3.12) to compute the branches of localized states. The continuation method we used can only find steady solutions, so the model is effectively the steady Swift–Hohenberg equation with solutions depending only on μ—though the stabilities depend on both μ and ν. The solutions are associated with homoclinic connections to the TS, in the same manner as spatially localized solutions in the Swift–Hohenberg equation (Burke & Dawes, 2012; Burke & Knobloch, 2006, 2007). The two localized branches with odd and even numbers of peaks add an oscillation on each side as they snake back and forth until they reach the width of the domain, where they terminate on the SS branch, at the saddle-node bifurcation (see Fig. 6). The localized solutions we obtained still exist but are unstable in the region where the TS becomes unstable, where $\mu < 0$ and $\nu > 0$.

From time-stepping, we also found LSS with an MW background in the region where the large-amplitude SS branch and the small-amplitude SW branch are both stable (see Figs 4, 5(*b*)).

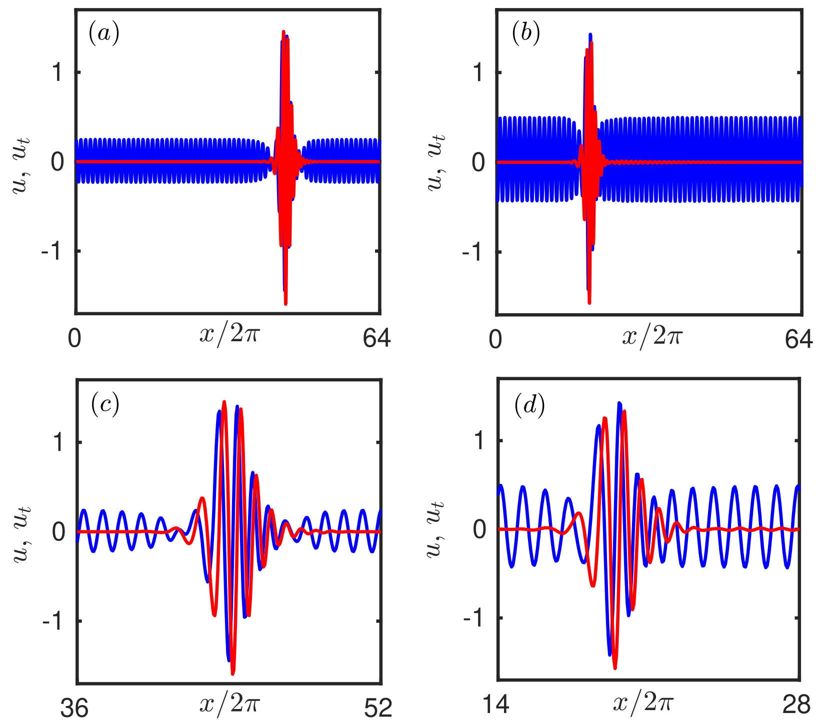

FIG. 10. Example of LTW with SS background (*a*) for radius 0.1 and $\theta = 170°$ (*b*) for radius 0.4 and $\theta = 160°$ where (*c*, *d*) are zooms of (*a*, *b*). The blue and red curves refer to u and u_t and the wave travels to the right. A movie of the state in (*a*) is available at Alrihieli *et al.* (2020).

In case I – with $A < 0$ and from time stepping, we found LTW with the TS background in the region where the TS and a large-amplitude branch of TW are stable, with $\mu < 0$ and $\nu < 0$ (see Fig. 8). We also found LTW with SS background in the region where the small-amplitude SS and large-amplitude TW are stable (see Figs 8 and 10). For the given parameter values, the LTW we found all have the same width, regardless of initial conditions. In contrast, LSS exist with a wide range of widths, with different numbers of peaks. In future work we will investigate why we get uniquely selected widths of LTW.

LTW-TS and with uniquely selected widths have also observed in experimental (Kolodner, 1991a,c, 1994; Niemela *et al.*, 1990) and numerical (Barten *et al.*, 1991, 1995b; Taraut *et al.*, 2012) studies of binary convection. These studies were not carried out close to the TB point, so our model does not directly apply here. Using continuation to compute the LTW solutions would need more effort due to the time and space dependence. The numerical continuation would then require additional unknown variables: the group velocity and the temporal period. An approach to solving this problem is suggested by Watanabe *et al.* (2011, 2012) and we plan to undertake this in future.

In this paper, we are interested in modelling systems such as thermosolutal (Da Costa *et al.*, 1981; Huppert & Moore, 1976; Moore *et al.*, 1991; Nield, 1967) and binary convection (Batiste & Knobloch, 2005; Knobloch, 1986; Knobloch & Moore, 1990; Watanabe *et al.*, 2012), where the pitchfork and Hopf bifurcations have the same critical wavenumbers (see Fig. 2), therefore, we assumed $k_{\mathrm{cPF}} = k_{\mathrm{cHopf}} = 1$. For future investigations, if $k_{\mathrm{cPF}} \neq k_{\mathrm{cHopf}}$ then this model could be relevant to other problems where the pitchfork and Hopf bifurcation have different critical wavenumbers, e.g. in magnetoconvection (Arter, 1983; Chandrasekhar, 1961; Clune & Knobloch, 1994; Dawes, 2000; Matthews & Rucklidge, 1993; Proctor & Weiss, 1982; Weiss, 1981) and rotating convection (Clune & Knobloch, 1993; Dawes, 2001; Veronis, 1966, 1968; Zimmermann *et al.*, 1988). In these cases, we might expect to find localized patterns with one wavenumber in a background of patterns with a different wavenumber, with either the localized state or the background pattern being time dependent. Finally, it would be interesting to explore pattern formation in this system for a wide range of parameters, both in 1D and 2D.

Acknowledgements

The authors would like to thank Cedric Béaume, Alan Champneys, Edgar Knobloch, David Lloyd, Jens Rademacher, Hermann Riecke and Arnd Scheel for many influential discussions.

Funding

PhD fellowship from Tabuk University in Saudi Arabia (H. A.); L'Oréal UK and Ireland Fellowship for Women in Science (P. S.); and Leverhulme Trust (RF-2018-449/9, A. M. R.).

References

Alrihieli, H., Rucklidge, A. M. & Subramanian, P. (2020) *Data for spatial localisation beyond steady states in the neighbourhood of the Takens–Bogdanov bifurcation*. Leeds: White Rose Repository. doi:10.5518/913.

Arter, W. (1983) Nonlinear convection in an imposed horizontal magnetic field. *Geophys. Astrophys. Fluid Dyn.*, **25**, 259–292.

Barten, W., Lücke, M. & Kamps, M. (1991) Localized traveling-wave convection in binary-fluid mixtures. *Phys. Rev. Lett.*, **66**, 2621.

Barten, W., Lücke, M., Kamps, M. & Schmitz, R. (1995a) Convection in binary fluid mixtures. I. Extended traveling-wave and stationary states. *Phys. Rev. E*, **51**, 5636.

Barten, W., Lücke, M., Kamps, M. & Schmitz, R. (1995b) Convection in binary fluid mixtures. *II. Localized traveling waves. Phys. Rev. E*, **51**, 5662.

Batiste, O., Knobloch, E., Alonso, A. & Mercader, I. (2006) Spatially localized binary-fluid convection. *J. Fluid Mech.*, **560**, 149–158.

Batiste, O. & Knobloch, E. (2005) Simulations of localized states of stationary convection in ^{3}He - ^{4}He mixtures. *Phys. Rev. Lett.*, **95**, 244501.

Beaume, C., Bergeon, A. & Knobloch, E. (2011) Homoclinic snaking of localized states in doubly diffusive convection. *Phys. Fluids*, **23**, 094102.

Beck, M., Knobloch, J., Lloyd, D. J. B., Sandstede, B. & Wagenknecht, T. (2009) Snakes, ladders. *and isolas of localized patterns. SIAM J. Math. Anal.*, **41**, 936–972.

Burke, J. & Dawes, J. H. P. (2012) Localized states in an extended Swift–Hohenberg equation. *SIAM J. Appl. Dyn. Syst.*, **11**, 261–284.

Burke, J. & Knobloch, E. (2006) Localized states in the generalized Swift–Hohenberg equation. *Phys. Rev. E*, **73**, 056211.

Burke, J. & Knobloch, E. (2007) Snakes and ladders: localized states in the Swift–Hohenberg equation. *Phys. Lett. A*, **360**, 681–688.

Canuto, C., Hussaini, M. Y., Quarteroni, A., Thomas Jr., A., et al. (2012) *Spectral Methods in Fluid Dynamics*. Berlin: Springer Science & Business Media.

Chandrasekhar, S. (1961) *Hydrodynamic and Hydromagnetic Stability*. Oxford: Clarendon Press.

Clune, T. & Knobloch, E. (1993) Pattern selection in rotating convection with experimental boundary conditions. *Phys. Rev. E*, **47**, 2536.

Clune, T. & Knobloch, E. (1994) Pattern selection in three-dimesional magnetoconvection. *Physica D*, **74**, 151–176.
Cox, S. M. & Matthews, P. C. (2002) Exponential time differencing for stiff systems. *J. Comput. Phys.*, **176**, 430–455.
Crawford, C. & Riecke, H. (1999) Oscillon-type structures and their interaction in a Swift–Hohenberg model. *Physica D*, **129**, 83–92.
Da Costa, L. N., Knobloch, E. & Weiss, N. O. (1981) Oscillations in double-diffusive convection. *J. Fluid Mech.*, **109**, 25–43.
Dangelmayr, G. & Knobloch, E. (1987) The Takens–Bogdanov bifurcation with O(2)-symmetry. *Phil. Trans. R. Soc. Lond. A*, **322**, 243–279.
Dawes, J. (2000) The 1:2 Hopf/steady-state mode interaction in three-dimensional magnetoconvection. *Physica D*, **139**, 109–136.
Dawes, J. (2001) A Hopf/steady-state mode interaction in rotating convection: bursts and heteroclinic cycles in a square periodic domain. *Physica D*, **149**, 197–209.
Deane, A. E., Knobloch, E. & Toomre, J. (1988) Traveling waves in large-aspect-ratio thermosolutal convection. *Phys. Rev. A*, **37**, 1817.
Doedel, E., Keller, H. B. & Kernevez, J. P. (1991) Numerical analysis and control of bifurcation problems (i): bifurcation in finite dimensions. *Int. J. Bifurc. Chaos*, **1**, 493–520.
Huppert, H. E. & Moore, D. R. (1976) Nonlinear double-diffusive convection. *J. Fluid Mech.*, **78**, 821–854.
Hussaini, M. Y. & Zang, T. A. (1987) Spectral methods in fluid dynamics. *Annu. Rev. Fluid Mech.*, **19**, 339–367.
Jung, D., Matura, P. & Lücke, M. (2004) Oscillatory convection in binary mixtures: thermodiffusion, solutal buoyancy. *and advection. Eur. Phys. J. E*, **15**, 293–304.
Jung, D. & Lücke, M. (2005) Traveling wave fronts and localized traveling wave convection in binary fluid mixtures. *Phys. Rev. E*, **72**, 026307.
Kassam, A.-K. & Trefethen, L. N. (2005) Fourth-order time-stepping for stiff PDEs. *SIAM J. Sci. Comput.*, **26**, 1214–1233.
Knobloch, E. (1986) Oscillatory convection in binary mixtures. *Phys. Rev. A*, **34**, 1538.
Knobloch, E., Moore, D. R., Toomre, J. & Weiss, N. O. (1986) Transitions to chaos in two-dimensional double-diffusive convection. *J. Fluid Mech.*, **166**, 409–448.
Knobloch, E. & Moore, D. R. (1990) Minimal model of binary fluid convection. *Phys. Rev. A*, **42**, 4693.
Knobloch, E. & Proctor, M. R. E. (1981) Nonlinear periodic convection in double-diffusive systems. *J. Fluid Mech.*, **108**, 291–316.
Kolodner, P. (1991a) Collisions between pulses of traveling-wave convection. *Phys. Rev. A*, **44**, 6466.
Kolodner, P. (1991b) Drift, shape, and intrinsic destabilization of pulses of traveling-wave convection. *Phys. Rev. A*, **44**, 6448.
Kolodner, P. (1991c) Stable and unstable pulses of traveling-wave convection. *Phys. Rev. A*, **43**, 2827.
Kolodner, P. (1994) Stable, unstable, and defected confined states of traveling-wave convection. *Phys. Rev. E*, **50**, 2731.
Kozyreff, G. & Tlidi, M. (2007) Nonvariational real Swift–Hohenberg equation for biological, chemical, and optical systems. *Chaos*, **17**, 037103.
Matthews, P. C. & Rucklidge, A. M. (1993) Travelling and standing waves in magnetoconvection. *Proc. R. Soc. London,. Series A*, **441**, 649–658.
Matura, P., Jung, D. & Lücke, M. (2004) Standing-wave oscillations in binary mixture convection: from the onset via symmetry breaking to period doubling into chaos. *Phys. Rev. Lett.*, **92**, 254501.
Mellibovsky, F. & Eckhardt, B. (2011) Takens–bogdanov bifurcation of travelling-wave solutions in pipe flow. *J. Fluid Mech.*, **670**, 96–129.
Mercader, I., Batiste, O., Alonso, A. & Knobloch, E. (2009) Localized pinning states in closed containers: homoclinic snaking without bistability. *Phys. Rev. E*, **80**, 025201.
Moore, D. R., Weiss, N. O. & Wilkins, J. M. (1991) Asymmetric oscillations in thermosolutal convection. *J. Fluid Mech.*, **233**, 561–585.

NIELD, D. A. (1967) The thermohaline Rayleigh–Jeffreys problem. *J. Fluid Mech.*, **29**, 545–558.

NIEMELA, J. J., AHLERS, G. & CANNELL, D. S. (1990) Localized traveling-wave states in binary-fluid convection. *Phys. Rev. Lett.*, **64**, 1365.

PROCTOR, M. R. E. & WEISS, N. O. (1982) Magnetoconvection. *Rep. Prog. Phys.*, **45**, 1317.

RUCKLIDGE, A. M. (1992) Chaos in models of double convection. *J. Fluid Mech.*, **237**, 209–229.

RUCKLIDGE, A. M. & SILBER, M. (2009) Design of parametrically forced patterns and quasipatterns. *SIAM J. Appl. Dyn. Syst.*, **8**, 298–347.

SPINA, A., TOOMRE, J. & KNOBLOCH, E. (1998) Confined states in large-aspect-ratio thermosolutal convection. *Phys. Rev. E*, **57**, 524.

SURKO, C. M., OHLSEN, D. R., YAMAMOTO, S. Y. & KOLODNER, P. (1991) Confined states of traveling-wave convection. *Phys. Rev. A*, **43**, 7101.

TARAUT, A. V., SMORODIN, B. L. & LÜCKE, M. (2012) Collisions of localized convection structures in binary fluid mixtures. *New J. Phys.*, **14**, 093055.

TURTON, S. E., TUCKERMAN, L. S. & BARKLEY, D. (2015) Prediction of frequencies in thermosolutal convection from mean flows. *Phys. Rev. E*, **91**, 043009.

VERONIS, G. (1965) On finite amplitude instability in thermohaline convection. *J. Mar. Res.*, **23**, 1–17.

VERONIS, G. (1966) Motions at subcritical values of the Rayleigh number in a rotating fluid. *J. Fluid Mech.*, **24**, 545–554.

VERONIS, G. (1968) Large-amplitude Bénard convection in a rotating fluid. *J. Fluid Mech.*, **31**, 113–139.

WATANABE, T., TOYABE, K., IIMA, M. & NISHIURA, Y. (2011) Time-periodic traveling solutions of localized convection cells in binary fluid mixture. *Theor. Appl. Mech. Japan*, **59**, 211–219.

WATANABE, T., IIMA, M. & NISHIURA, Y. (2012) Spontaneous formation of travelling localized structures and their asymptotic behaviour in binary fluid convection. *J. Fluid Mech.*, **712**, 219–243.

WEISS, N. O. (1981) Convection in an imposed magnetic field. Part 1. The development of nonlinear convection. *J. Fluid Mech.*, **108**, 247–272.

ZHAO, B. & TIAN, Z. (2015) Numerical investigation of binary fluid convection with a weak negative separation ratio in finite containers. *Phys. Fluids*, **27**, 074102.

ZIMMERMANN, W., ARMBRUSTER, D., KRAMER, L. & KUANG, W. (1988) The effect of spatial modulations on codimension-2 bifurcations. *Europhys. Lett.*, **6**, 505.